

Electronic Structure of Mononuclear Cu-based Molecule from Density-Functional Theory with Self-Interaction Correction

Anri Karanovich,¹ Yoh Yamamoto,² Koblar Alan Jackson,³ and Kyungwha Park^{1, a)}

¹⁾*Department of Physics, Virginia Tech, Blacksburg, Virginia 24061, USA*

²⁾*Department of Physics, University of Texas at El Paso, El Paso, Texas 79968, USA*

³⁾*Physics Department and Science of Advanced Materials Program, Central Michigan University, Mt. Pleasant, Michigan 48859, USA*

(Dated: 7 February 2022)

We investigate the electronic structure of a planar mononuclear Cu-based molecule $[\text{Cu}(\text{C}_6\text{H}_4\text{S}_2)_2]^z$ in two oxidation states ($z=-2, -1$) using density-functional theory (DFT) with Fermi-Löwdin orbital (FLO) self-interaction correction (SIC). The dianionic Cu-based molecule was proposed to be a promising qubit candidate. Self-interaction error within approximate DFT functionals renders severe delocalization of electron and spin densities arising from $3d$ orbitals. The FLO-SIC method relies on optimization of Fermi-Löwdin orbital descriptors (FODs) with which localized occupied orbitals are constructed to create the SIC potentials. Starting with many initial sets of FODs, we employ a frozen-density loop algorithm within the FLO-SIC method to study the Cu-based molecule. We find that the electronic structure of the molecule remains unchanged despite somewhat different final FOD configurations. In the dianionic state (spin $S = 1/2$), FLO-SIC spin density originates from the Cu d and S p orbitals with an approximate ratio of 2:1, in quantitative agreement with multireference calculations, while in the case of SIC-free DFT, the orbital ratio is reversed. Overall, FLO-SIC lowers the energies of the occupied orbitals and in particular the $3d$ orbitals unhybridized with the ligands significantly, which substantially increases the energy gap between the highest occupied molecular orbital (HOMO) and the lowest unoccupied molecular orbital (LUMO) compared to SIC-free DFT results. The FLO-SIC HOMO-LUMO gap of the dianionic state is larger than that of the monoionic state, which is consistent with experiment. Our results suggest a positive outlook of the FLO-SIC method in the description of magnetic exchange coupling within $3d$ -element based systems.

I. INTRODUCTION

Systems including $3d$ transition-metal elements are difficult to study using density-functional theory (DFT) due to strong electron correlation involving the localized d orbitals. The approximate nature of the exchange-correlation functional within the DFT formalism limits an accurate description of multiconfigurational/multireference features of strongly correlated systems. In addition, such nature allows significant Coulomb interactions of electrons with themselves, referred to as self-interaction error (SIE)¹, which results in an underestimate of the band gap or gap between the highest occupied molecular orbital (HOMO) and the lowest unoccupied molecular orbital (LUMO) as well as an overestimate of exchange interaction between $3d$ transition-metal centers, to name a few. An introduction of on-site Coulomb repulsion U within the DFT formalism^{2,3} aligns with an effort to compensate for SIE. Although standard multireference quantum chemistry methods can describe mononuclear transition-metal-based molecules, they are not practical for multinuclear magnetic molecules due to extremely high computational cost.

As an alternative, one can consider an application of DFT with self-interaction correction (SIC) to $3d$

transition-metal systems. Perdew and Zunger (PZ) proposed a systematic method to impose the SIC to any spin-density-functional approximation¹. This PZ-SIC formalism was successfully applied within the local spin density approximation (LSDA) to atoms and molecules^{1,4} and solids⁵. However, the PZ-SIC method adds a set of N^2 conditions that need to be satisfied to reach a minimum energy and the SIC energy is not necessarily size-consistent, where N is the total number of electrons. Recently, a new practical SIC scheme adapted from the PZ-SIC formalism has been proposed using localized Fermi-Löwdin orbitals (FLO)^{6,7}. In this scheme referred to as FLO-SIC, $3N$ conditions have to be satisfied and the SIC energy is size-consistent. The FLO-SIC method was applied to various non-magnetic molecules⁸⁻¹⁴, giving rise to improvement of ionization energies of organic molecules⁹ and vertical detachment energies of water clusters¹⁰. However, applications of the FLO-SIC method to $3d$ transition-metal systems have been limited^{11,13,15}. Small mononuclear $3d$ transition-metal-based molecules would be ideal to gauge an applicability of the FLO-SIC method, the results of which provide insight into employment of the FLO-SIC method to multinuclear $3d$ transition-metal systems.

Recently, a crystal of small Cu-based magnetic molecules, $[\text{Cu}(\text{C}_6\text{H}_4\text{S}_2)_2]^{-2}$ (or $[\text{Cu}(\text{II})(\text{bdt}^{2-})_2]^{-2}$), has been shown to have long spin-lattice and spin-spin relaxation times at room temperature attributed to small spin-orbit coupling, to the well-separated ground doublet, and

^{a)}Electronic mail: kyungwha@vt.edu (corresponding author)

to strong metal-ligand covalency¹⁶, which renders the molecule a promising candidate for quantum information science applications. The electronic structure of the dianionic Cu-based molecule was investigated using electron paramagnetic resonance (EPR) experiments^{16,17}, and it was also calculated using multireference quantum chemistry methods¹⁶, time-dependent DFT (TDDFT)¹⁷, and DFT with a hybrid functional¹⁷. Interestingly, Ref. 17 suggested that two competing electronic structures (where the spin density is mostly carried by either the Cu or the S ligands) coexist in the dianionic Cu-based molecule, although such a scenario was not reported in the multireference study¹⁶. On the other hand, the monoanionic Cu-based molecule, $[\text{Cu}(\text{C}_6\text{H}_4\text{S}_2)_2]^{1-}$, was observed to be non-magnetic with its UV-visible absorption peak at somewhat lower energy than the dianionic molecule¹⁷. Derivatives of the monoanionic Cu-based molecule were also synthesized and their properties including optical absorption spectra were characterized^{18,19}. The electronic structures of the monoanionic molecule and one of the derivatives, $[\text{Cu}(\text{III})(\text{C}_{14}\text{H}_{20}\text{S}_2)_2]^{1-}$, were calculated using DFT with a hybrid functional^{17,18}.

In this work, we systematically investigate the electronic structure of the dianionic and monoanionic mononuclear Cu-based molecules, $[\text{Cu}(\text{C}_6\text{H}_4\text{S}_2)_2]^z$ ($z = -2, -1$), using the FLO-SIC method. Starting with many Fermi-Löwdin orbital descriptor (FOD) configurations for a given molecular structure and charge state, we optimize them in order to obtain the optimal FLO-SIC energy for each FLO configuration. For comparison, we also do SIC-free (standard) DFT and self-interaction free wave function calculations at the unrestricted Hartree-Fock (UHF) and multiconfigurational levels. Since the FLO-SIC potential lowers energies of the occupied Cu d orbitals much more than the occupied ligand orbitals, the FLO-SIC HOMO energy is greatly shifted downward which results in a large HOMO-LUMO gap. In addition, characteristics of the FLO-SIC HOMO significantly differ from those of the standard DFT and multiconfigurational/multireference calculations. The FLO-SIC spin density for the dianionic case quantitatively agrees well with the multiconfigurational/multireference result and it is consistent with EPR experimental data¹⁷. The FLO-SIC HOMO-LUMO gap of the monoanionic molecule is significantly smaller than that of the dianionic molecule, which may be in line with the experimental UV-optical absorption spectra.

In Sec. II we present the geometries of the dianionic and monoanionic Cu-based molecules that we use. In Sec. III we discuss our systematic applications of the FLO-SIC method to the molecules using a frozen-density loop algorithm, molecular symmetries and previous FLO-SIC results from atoms²⁰. Then we show the FLO-SIC charge and spin density of states as well as the HOMO and LUMO characteristics for the two charge states compared to our UHF, standard (SIC-free) DFT, and multiconfigurational calculations as well as other groups'

studies^{16–18} in Secs. IV and V. In Sec. VI we make conclusions and provide outlook.

II. GEOMETRIES OF CU-BASED MOLECULES

Figure 1 shows the molecular geometry of $[\text{Cu}(\text{C}_6\text{H}_4\text{S}_2)_2]^{2-}$ (referred to as **Q-2**) derived from the experimental data¹⁷. The molecule has almost planar structure in the xy plane with inversion symmetry up to precision of $\sim 10^{-4}\text{\AA}$. There is an approximate D_{2h} symmetry. The Cu-S bond lengths are 2.294 and 2.265 Å, and the S-Cu-S angles are 89.6 and 90.4°. A nominal ionic picture dictates that the Cu^{2+} ion ($3d^9$) carries the spin $S = 1/2$, while the four S atoms, each of which has an oxidation state of -1 , do not carry spin. However, the experimental data^{16,17} strongly suggests covalent bonding between the Cu and the S atoms. In our study, we use the experimental geometry of **Q-2**¹⁷ with C-H bond lengths modified to be a standard value of 1.09 Å, without further geometry relaxation. The coordinates of the molecular geometry are listed in Table VI in the Appendix A.

The experimental geometry of the monoanionic molecule, $[\text{Cu}(\text{C}_6\text{H}_4\text{S}_2)_2]^{1-}$ (referred to as **Q-1**), is not available. Therefore, we separately optimize the molecular geometry of **Q-1** for the triplet ($S = 1$) and singlet state ($S = 0$) without symmetry constraints until the root mean square of the force is less than 1 mHa/ a_B (where a_B is Bohr radius) within the Perdew-Burke-Ernzerhof (PBE) generalized-gradient approximation (GGA)²¹ using the NRLMOL code^{22–24}. Our DFT calculation without SIC shows that the singlet state has a lower energy than the triplet state (by 0.39 eV). This trend agrees with the literature¹⁷. The optimized singlet structure has slightly reduced Cu-S bond lengths such as 2.223 and 2.228 Å (compared to those for **Q-2**) with the S-Cu-S angles of 89.3 and 90.7°. An experimental crystallographic data on a similar monoanionic Cu-based molecule, $[\text{Cu}(\text{C}_{14}\text{H}_{20}\text{S}_2)_2]^{1-}$ suggests that the Cu-S bond lengths are 2.16 and 2.17 Å in the singlet state¹⁸, which agrees with the reported experimental Cu-S bond lengths in **Q-1**¹⁷. In our study, we use the PBE-GGA-optimized geometry for **Q-1** that has inversion symmetry up to the precision of $\sim 10^{-4}\text{\AA}$ and approximate D_{2h} symmetry. The coordinates of the optimized geometry are listed in Table VII in the Appendix A.

III. FLO-SIC METHODS

A. FLO-SIC formulation

In order to include the SIC in an approximate exchange-correlation energy $E_{xc}^{\text{app}}[n_{\uparrow}, n_{\downarrow}]$, Perdew and Zunger¹ considered the following self-interaction cor-

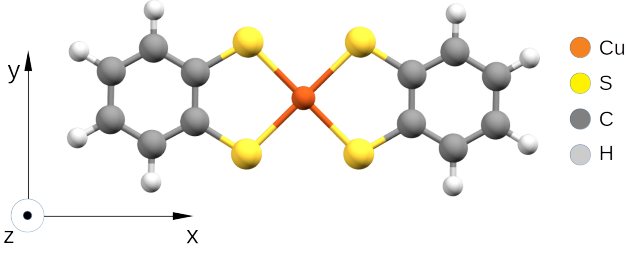


FIG. 1. Molecular geometry of $[\text{Cu}(\text{C}_6\text{H}_4\text{S}_2)_2]^{2-}$ (**Q-2**) from the experimental data¹⁷. The molecule is almost planar in the xy plane. **Q-1** has a similar molecular geometry to **Q-2**.

rected exchange-correlation energy $E_{\text{xc}}^{\text{SIC}}$:

$$E_{\text{xc}}^{\text{SIC}} = E_{\text{xc}}^{\text{app}}[n_{\uparrow}, n_{\downarrow}] - \sum_{i,\sigma} (U^{\text{s}}[n_{i\sigma}] + E_{\text{xc}}^{\text{app}}[n_{i\sigma}, 0]), \quad (1)$$

$$n_{\sigma}(\mathbf{r}) = \sum_i |\phi_{i\sigma}(\mathbf{r})|^2 = \sum_{\alpha} |\psi_{\alpha\sigma}(\mathbf{r})|^2, \quad (2)$$

where $\phi_{i\sigma}(\mathbf{r})$ and $\psi_{\alpha\sigma}(\mathbf{r})$ are localized occupied orbitals and canonical (Kohn-Sham) orbitals, respectively, and $n_{i\sigma=\uparrow,\downarrow}(\mathbf{r}) = |\phi_{i\sigma}(\mathbf{r})|^2$. By definition, the self-direct Coulomb energy $U^{\text{s}}[n_{i\sigma}]$ of a single fully occupied electron must completely cancel its exact exchange-correlation energy $E_{\text{xc}}[n_{i\sigma}, 0]$. However, the exact cancellation is not achieved within approximate exchange-correlation functionals, and Eq. (1) takes care of the incomplete cancellation. The SIC energy $E_{\text{xc}}^{\text{SIC}}$ depends on both the electron density and the orbitals rather than just the electron density.

In the FLO-SIC method^{6,7,25}, in order to maintain unitary invariance of the SIC energy with respect to orbital transformations, Eq. (1), a set of Fermi orbitals $F_{i\sigma}(\mathbf{r})$ are constructed from an initial set of Kohn-Sham orbitals $\psi_{\alpha\sigma}(\mathbf{r})$ as follows:

$$F_{i\sigma}(\mathbf{r}) = \frac{\sum_{\alpha} \psi_{\alpha\sigma}(\mathbf{a}_{i\sigma}) \psi_{\alpha\sigma}(\mathbf{r})}{\sqrt{\sum_{\alpha} |\psi_{\alpha\sigma}(\mathbf{a}_{i\sigma})|^2}}, \quad (3)$$

where the index i runs over all occupied orbitals. Here $\mathbf{a}_{i\sigma}$ are three-dimensional spatial coordinates assigned to each occupied orbital i with spin σ , which are referred to as Fermi-orbital descriptor (FOD). Unitary invariance is assured since any set of orthonormal orbitals that span the occupied space can be used in Eq. (3). Note that chemical properties of systems are reflected in the optimized FODs. Equation (3) ensures localization and the Löwdin scheme²⁶ guarantees orthonormality of orbitals. The constructed orbitals are referred to as Fermi-Löwdin orbitals (FLO). The localized orbitals are used to ensure size consistency of the SIC energy. The total energy including the SIC energy must be minimized both with respect to the density, through standard self-consistent calculations, and with respect to FOD positions.

The FLO-SIC calculations are performed using the FLOSIC 0.2 program²⁷, which is based on the NRLMOL

code²²⁻²⁴. We use the Gaussian-type basis sets optimized by Pederson and Porezag²⁸. Typically, a SIC-free DFT calculation within the L(S)DA-PW92²⁹ or PBE-GGA exchange-correlation functional is first carried out to obtain the converged electron density and an initial set of Kohn-Sham orbitals. Then for the given electron density, an initial set of FLOs is constructed using the Kohn-Sham orbitals and an initial set of FODs [Eq. (3)]. Next the SIC energy is computed and the electron density is updated in a self-consistent-field (SCF) loop within the L(S)DA-PW92 exchange-correlation functional including the one-electron SIC potentials. Using the updated electron density, the set of the FOD positions is updated with a gradient-based optimization algorithm using analytic FOD forces⁷. This procedure is repeated until the total energy including the SIC energy reaches a minimum and the maximum force on the FODs is less than a tolerance.

B. Frozen-density loop method

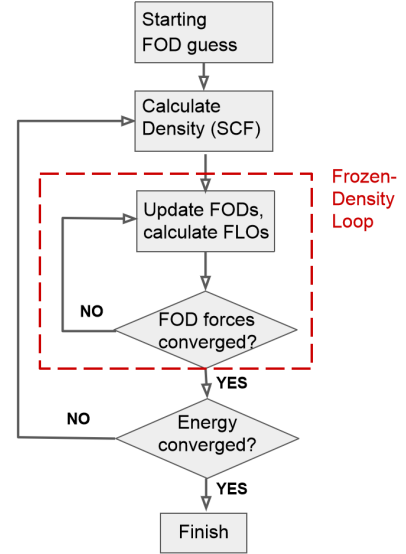


FIG. 2. Schematic flow chart of the frozen-density loop procedure within the FLO-SIC method.

For large molecules especially including transition-metal elements, many starting sets of FODs may need to be considered in FLO-SIC calculations, and the convergence of the total energy with respect to the FODs is known to be much slower than the electronic convergence of a SIC-free DFT SCF run. Therefore, there is a great demand for expediting FLO-SIC calculations. We apply the following modification to the FLO-SIC method. Instead of re-optimizing the electron density within a SCF loop after every FOD update, the density is held fixed (frozen) while the SIC energy is minimized with respect to FOD positions only. When the FOD geometry converges with the given FOD force tolerance (0.5 mHa/ a_B) in our calculations, the electron density is recalculated

self-consistently with the new converged FOD positions, and the procedure is repeated until the total energy converges. In this method referred to as frozen-density loop algorithm (Fig. 2), a full FOD optimization is performed for each SCF density. We find the frozen density scheme to be significantly more efficient, saving up to a factor of six in total computational effort for the dianionic Cu-based molecule consisting of 175 electrons. The saving does not result from a decrease in the number of steps in the gradient optimization of the FODs, which is roughly the same in each approach. Instead, it derives from a much smaller number of SCF steps taken in the frozen density approach.

C. Starting sets of FODs for the Q-2 molecule

Multiple local minima in total energy may be possible in the FOD optimization²⁰. In order to ensure that we reach the minimum-energy FOD configuration, we consider multiple starting sets of FODs described in this subsection. Since the number of three-dimensional FOD position vectors equals the number of electrons, we need 175 initial FOD vectors for the **Q-2** molecule which consists of 88 spin-up (majority-spin) and 87 spin-down (minority-spin) FODs. Previous FLO-SIC studies showed that starting sets of FODs of ligands (i.e., *s*- and *p*-electron systems) generated by the Monte-Carlo-based fodMC code¹⁴ converge rapidly to the minimum SIC energy, whereas effectiveness of the fodMC code for transition-metal systems is not guaranteed. FOD positions associated with or around the transition-metal centers are also known to converge extremely slowly despite the fact that these FOD forces are largest. Therefore, for the starting sets of FODs, it makes sense to treat Cu and ligand FODs separately.

We assign the initial FODs of the ligands using the fodMC code. Considering the Cu-S bonding, we place four spin-up and four spin-down FODs at the same positions along the Cu-S bonding directions. This assignment is consistent with the majority of the spin density from the Cu center. There is one ambiguity related to the delocalized *p*-electrons on the benzene-like rings. One obvious way to put FODs there is to follow a classical single-double bond picture, and assign one FOD of each species to each single bond and two FODs to each double bond. Another way is to alternate, such that one C-C bond in the ring has 2 spin-up FODs and 1 spin-down FOD, and the next bond has 1 spin-up FOD and 2 spin-down FOD. The latter alternating picture is related to Linnett double-quartet theory and has been shown to achieve slightly lower energy than the former scheme³⁰. Therefore, the alternating FOD pattern is used for the ligands. These starting ligand FODs are used for all the FOD configurations of the same charge state, which differ only in the Cu starting FODs.

Since the fodMC program does not guarantee good starting FOD positions for transition-metal centers, a dif-

ferent strategy should be used. One possibility is to use a set of pre-converged single-atom results by Kao et.al²⁰. Although this could be a good starting point, it has several disadvantages. Firstly, the electronic structure of the bonded, oxidized atom differs from that of an isolated one, and so significant re-optimization of the starting positions may be expected. Secondly, it is not clear which FODs from the optimized neutral atom should be removed to create the expected oxidation state. Finally, this approach provides few possibilities to systematically probe the space of initial FOD geometries.

Another, more systematic approach is based on the following considerations. It is known from single-atom results²⁰ that FODs tend to group by the principal quantum numbers of orbitals they represent. For instance, in Ar atom, for each spin channel there is one FOD at the center corresponding to 1*s* orbital, 4 FODs in a shape of tetrahedron centered at the atom (for 2*s* and 2*p* orbitals), and another 4 FODs in a tetrahedron but of larger dimensions for 3*s* and 3*p* orbitals. The molecular symmetry needs to be reflected in the initial FOD geometries. Considering that the Cu-S bond angles are close to 90°, there is an approximate 4-fold rotational symmetry of Cu atom with respect to Cu-S bonds.

Based on the above considerations, the following procedure is used for systematic generation of 12 initial Cu FODs (see Fig. 3):

- Identify three groups of FODs around the Cu center, distinct by their distances to the center, following the single-atom Cu FOD result²⁰.
- Using these distances, consider the following number of FODs at concentric spherical shells: 1 spin-up and 1 spin-down FOD at the center ($n = 1$); 4 spin-up and 4 spin-down FODs at a smaller ($n = 2$) sphere; and 9 spin-up and 8 spin-down at the larger ($n = 3$) sphere.
- Place these FODs in a 4-fold symmetric fashion as shown in Fig. 3. For the $n = 2$ shell, 4 FODs are placed at the vertices of opposing tetrahedra, in each of which two edges are parallel to the molecular plane either oriented along the *x* and *y* axes or along the diagonals (i.e. Cu-S bonds); For the $n = 3$ shell, 4 FODs are above the molecular plane, forming a square, while 4 FODs are below the plane in a rhombus, with 1 spin-up FOD directly on top of the Cu site.

D. Starting sets of FODs for the Q-1 molecule

For generation of initial FODs for the **Q-1** molecule, a similar scheme to that of the **Q-2** molecule is used. The initial Cu FODs that we consider are shown in Fig. 4. Since the **Q-1** molecule is in a singlet state, we perform spin-unpolarized FLO-SIC calculations, where spin-up and spin-down FODs must occupy the same positions.




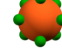



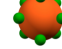






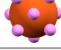
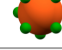
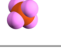


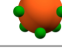
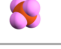


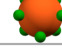
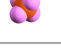

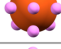

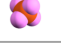






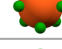


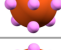
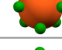








FOD Conf.	n=2 shell		n=3 shell	
	spin-up	spin-dn	spin-up	spin-dn
1				
2				
3				
4				
5				
6				
7				
8				
9				
10				
11				
12				

FIG. 3. Schematic depiction of 12 starting FOD geometries associated with Cu in the **Q-2** molecule. Orange spheres represent concentric spheres around the Cu atom where magenta (green) dots are for spin-up (spin-down) FODs.








FOD Conf.	n=2 shell	n=3 shell
1		
2		
3		
4		

FIG. 4. Schematic depiction of 4 starting spin-unpolarized FOD geometries associated with Cu in the **Q-1** molecule. Orange spheres represent concentric spheres around the Cu atom where magenta dots are for FODs.

This reduces the number of FODs and computational time by half. The results shown in Sec. V are obtained using spin-unpolarized FLO-SIC calculations. In all other aspects, the procedure on the **Q-1** is the same as on the **Q-2** molecule.

IV. FLOSIC RESULTS FOR THE Q-2 MOLECULE

A. Converged FODs and energy convergence

For the 12 starting FOD configurations (Fig. 3) with the same DFT-converged electron density, FLO-SIC calculations are carried out using the frozen-density loop method (Fig. 2). After the first frozen-density loop cycle, converged FODs starting from configuration 9-12 are found to have similar total energies and similar FOD positions to FOD configuration 1-4, respectively. After the second frozen-density loop cycle, FOD configuration 1 is found to reach the same converged energy and same FOD positions as FOD configuration 4. Therefore, we continue to relax the FOD positions and the electron density only for the remaining 7 FOD configurations (configuration 2-8). After completion of 6 cycles of the frozen-density loop, we find that the SCF total energy converges within below or up to 1 mHa. Figure 5 shows the convergence of the SCF total energy versus FOD iteration number for configuration 2-5. The sudden drops in the energy correspond to switches between frozen-density loop cycles. Although different FOD configurations converge at different rates, configuration 2-4 seem to converge to the same total energy.

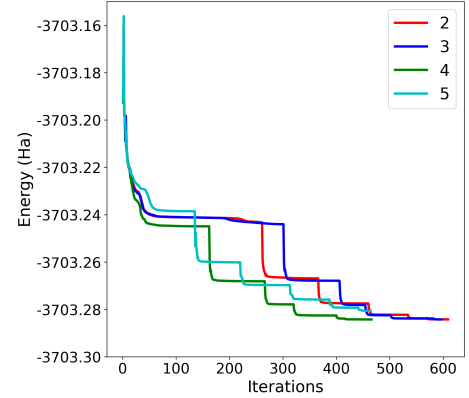


FIG. 5. Total energy versus FOD update or iteration number for FOD configuration 2-5 (labeled in Fig. 3) of the **Q-2** molecule. After the initial steep relaxation of the energy, the step-function-like abrupt jump occurs whenever the electron density is updated after each frozen-density loop converges. Here 6 frozen-density loop cycles are shown.

The total energy changes by about 1 mHa or less than 1 mHa after the 6-th frozen-density loop cycle compared to the energy after the 5-th cycle (see the ΔE values in Table I). Therefore, we analyze our FLO-SIC results us-

TABLE I. Converged SCF total energies E and maximum final force components F_{\max} after the 6 frozen-density loops, and energy differences ΔE between the 6-th and 5-th frozen-density loop cycles for the configuration 2-8 (labeled in Fig. 3) of the **Q-2** molecule. Each frozen-density loop cycle consists of many FOD updates. For example, for the FOD configuration 2, there are 609 updates or iterations of the FODs after the 6 frozen-density loop cycles.

FOD Conf	E (Ha)	F_{\max} (mHa/ a_B)	ΔE (mHa)
2	-3703.28420	0.48	-0.43
3	-3703.28421	0.48	-0.37
4	-3703.28422	0.36	-0.35
5	-3703.28054	0.37	-1.30
6	-3703.28189	0.32	-0.53
7	-3703.28401	0.42	-0.77
8	-3703.28273	0.39	-0.60

ing the data obtained after the 6-th cycle. Each cycle consists of many FOD updates or iterations as shown in Fig. 5. Table I lists the converged total energies and maximum force components after the 6 frozen-density loop cycles. FOD configuration 4 gives the lowest energy, but the energy differences among the different FOD configurations are on the order of mHa at most. The maximum force component F_{\max} is about 0.3-0.5 mHa/ a_B , while the maximum electric dipole moment component is about 0.006-0.007 in atomic units (and the maximum dipole moment component from the SIC-free PBE-GGA is about 0.001 in atomic units).

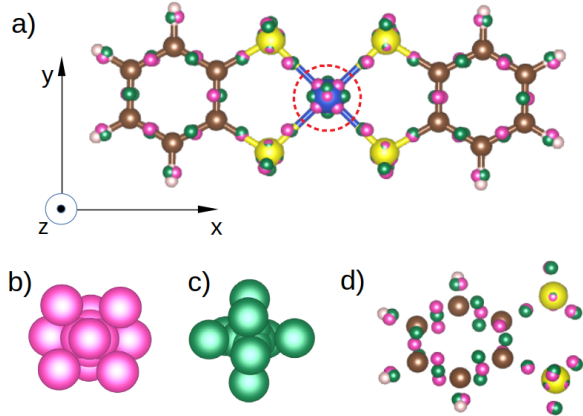


FIG. 6. (a) Final converged FOD positions for configuration 4 of the **Q-2** molecule with magenta (green) color for spin-up (spin-down) FODs. (b) and (c) Zoom-in of the spin-up and spin-down FODs near the Cu atom. (d) Zoom-in of the spin-up and spin-down FODs near the ligands. The zoom-in region is indicated as a red dashed circle in (a).

Figure 6 shows the converged FOD positions of configuration 4 after the 6-th frozen-density loop cycle. The initial spin-down FOD positions significantly change upon relaxation compared to the initial spin-up FOD positions.

The converged spin-up and spin-down FOD positions (starting from configuration 4) are listed in Tables VIII and IX in the Appendix C 1. Henceforth, we examine the FLO-SIC calculated electronic structure of the molecule using the electron density obtained from this converged FOD configuration. We confirm that the FLO-SIC electronic structure from the other converged FOD configurations 2, 3, 5, 6, 7, and 8 is very close to that from the converged FOD configuration 4, within our numerical accuracy (Table XI in the Appendix), although the final configurations of the core and valence FODs somewhat differ from one another. We also check that the electronic structure does not change with further relaxations of the FODs beyond the threshold and/or with further decrease of the electric dipole moment.

B. FLOSIC-calculated electronic structure

Using the FLO-SIC result, we calculate Mulliken spin populations of the Cu atom, all four S atoms, and all C atoms of the **Q-2** molecule ($S = 1/2$). We find that the majority of the spin density (67%) arises from the Cu center and the rest from the S atoms (33%) and from the C atoms (-3%). These FLO-SIC calculated values are close to the values from our UHF calculation (Table II). Although electron correlation is not included in the UHF calculation, there is no SIE in it. Therefore, this indicates that the SIC is properly taken care of in our FLO-SIC calculation. The FLO-SIC spin populations are also close to our multiconfigurational complete active space self-consistent field (CASSCF) result, as well as a previous multireference result¹⁶ based on complete active space second-order perturbation theory (CASPT2). Since CASPT2 includes both static and dynamic correlations, our FLO-SIC result is very encouraging. The detail of our CASSCF and UHF calculations is described in the Appendix B.

Now we compare the FLO-SIC spin populations to those from our SIC-free DFT calculations (Table II). Both LSDA-PW92 and PBE-GGA exchange correlation functionals without the SIC give rise to much more delocalized spin density with a large contribution from the S atoms (about 70%) and a much smaller contribution from the Cu center (about 30%).

We compute the energy levels of the HOMO and LUMO using the FLO-SIC result (see Table III) for the **Q-2** molecule, finding that the HOMO energy is negative. This indicates that the dianionic form of the molecule can exist, which is consistent with the experimental synthesis of the dianionic **Q-2** molecule^{16,17}. The SIC-free PBE-GGA calculation provides a positive HOMO energy. The comparison between the FLO-SIC and the SIC-free DFT results shows that the SIC shifts the HOMO level downward by 5.07 eV, while it shifts the LUMO level upward by 0.71 eV. The FLO-SIC HOMO-LUMO gap is about 6.34 eV, while the corresponding gap from the SIC-free DFT is about 0.57 eV. Since the SIC potential energy is

TABLE II. Calculated Mulliken spin populations of the Cu and all four S atoms (in units of Bohr magneton μ_B) of the **Q-2** molecule ($S = 1/2$) using different levels of computational methods. In the CASPT2 calculation¹⁶, the C spin population was not reported, while in the EPR experiment¹⁷, only the spin density from the Cu d_{xy} orbital was reported. The Cu, S, and C spin populations from the FLO-SIC and SIC-free DFT calculations do not add up to 1.00 μ_B due to very small spin populations on the H atoms. All of the values are our results unless specified otherwise.

Method	Cu	S	C
FLO-SIC	0.67	0.33	-0.03
Unrestricted Hartree Fock	0.79	0.22	-0.01
CASSCF(11,11)	0.70	0.29	0.01
CASPT2 (Ref.16)	0.76	0.24	N/A
SIC-free DFT (LSDA-PW92)	0.31	0.72	-0.08
SIC-free DFT (PBE-GGA)	0.32	0.73	-0.12
B3LYP DFT (Ref.17)	0.24	0.76	0.00
EPR experiment (Ref.17)	0.51	N/A	N/A

typically negative, it lowers the energies of the occupied orbitals. As a result, the HOMO-LUMO gap increases with the SIC. The small change of the LUMO level with the SIC is due to the orbital relaxation effect.

TABLE III. Contributions of the Cu d , all S p , and all C p orbitals to the HOMO and LUMO of the **Q-2** (charge $Q = -2$, $S = 1/2$) molecule calculated using the FLO-SIC method in comparison to our SIC-free PBE-GGA calculations as well as an earlier B3LYP result¹⁷ where the orbital decomposition was not reported. In our calculations (PBE-GGA, FLO-SIC), the HOMO arises from the spin-up (majority-spin) orbital and the LUMO from the spin-down (minority-spin) orbital (see Fig. 7), while in the B3LYP calculation¹⁷, both HOMO and LUMO are from the spin-down orbitals.

Method	Level	Energy(eV)	Cu d	S p	C p
FLO-SIC	HOMO	-1.99	2.2%	74%	23%
	LUMO	4.35	85%	11%	0.5%
PBE-GGA	HOMO	3.08	49%	46%	1.4%
	LUMO	3.65	57%	37%	1.5%
B3LYP ¹⁷	HOMO	~3.3	-	-	-
	LUMO	~5.3	-	-	-

Figure 7 shows the HOMO and LUMO and a few other *canonical* orbitals of the **Q-2** molecule calculated from the FLO-SIC method in comparison to the PBE-GGA orbitals. The FLO-SIC HOMO looks similar to the SIC-free DFT HOMO-2, while the FLO-SIC HOMO-2 looks similar to the SIC-free DFT HOMO. The other occupied orbitals do not seem to change their overall shapes other than the energies and Cu contributions. Table III lists quantitative characteristics of the HOMO and LUMO using the FLO-SIC method and the PBE-GGA. The FLO-SIC calculation shows that the HOMO arises mainly from the spin-up S $p_{x,y}$ orbitals with significant contributions from the spin-up C $p_{x,y}$ orbitals and a tiny contribution from the spin-up Cu d_{xy} orbitals, whereas the LUMO

consists of a major contribution from the spin-down Cu d_{xy} and some contributions from the spin-down S $p_{x,y}$ orbitals. These orbital characteristics are very different from those obtained using the SIC-free DFT. For the latter, both the HOMO and LUMO consist of large contributions from the Cu d_{xy} and S $p_{x,y}$ orbitals. The FLO-SIC LUMO and the SIC-free DFT HOMO and LUMO shown in Fig. 7 can be identified as antibonding orbitals which are combinations of the Cu d_{xy} and the S $p_{x,y}$ orbitals. The CASSCF calculation shows that the singly occupied active orbital of the lowest-energy configuration has the character of the majority-spin (spin-up) Cu-S antibonding orbital (molecular orbital 6 in Fig. 12) and it can be viewed as the HOMO at the single-electron picture.

In order to understand the effect of FLO-SIC on the HOMO and other occupied orbitals, we plot the densities of states (DOS) projected onto spin-up and spin-down Cu d , S p , and C p orbitals, as shown in Fig. 8. From the comparison between the FLO-SIC and the SIC-free DFT DOS plots, we find that the SIC lowers the occupied S p and C p orbitals by about 5 eV and the occupied Cu spin-up $3d$ orbitals by about 14-15 eV. The SIC effect is expected to be stronger for the $3d$ orbitals than for the p orbitals since the $3d$ orbitals are more strongly localized, i.e., larger self-interaction energy in the SIC-free DFT result. The highest occupied spin-down Cu d orbital energy is lowered by only about 6.5 eV, which is much smaller than the case of the corresponding spin-up orbital energy due to hybridization of the spin-down Cu orbital with the spin-down S p orbital. This is consistent with the PZ-SIC results of the $3d$ transition metal atoms¹ which are attributed to a more attractive exchange-correlation potential seen by the spin-up $3d$ orbitals. The characteristics of the HOMO qualitatively changes with the SIC because of the much larger downward shift of the spin-up Cu d orbitals than the S p orbitals.

C. Comparison with previous work

Experimental data¹⁶ on the **Q-2** molecule indicates a strong covalent nature of Cu-S bonding which leads to long spin relaxation and coherence times. EPR experiments¹⁷ imply that about 51% of the spin density arises from the Cu d_{xy} orbitals for **Q-2**. The CASPT2 calculation from Ref. 16 shows that 76% (24%) of the spin density originates from the Cu (S) atoms. Both the experimental data and the CASPT2 result suggest a majority contribution of the Cu d orbitals to the spin density, which is in line with our FLO-SIC and CASSCF spin populations. Especially, the CASPT2¹⁶ and our CASSCF spin populations quantitatively agree with our FLO-SIC values (see Table II).

However, recent DFT calculations¹⁷ using a hybrid functional such as Becke, 3-parameter, Lee-Yang-Parr (B3LYP)³¹⁻³⁴, indicate that the Cu d (S p) orbitals carry 24% (76%) of the total spin density and that both the

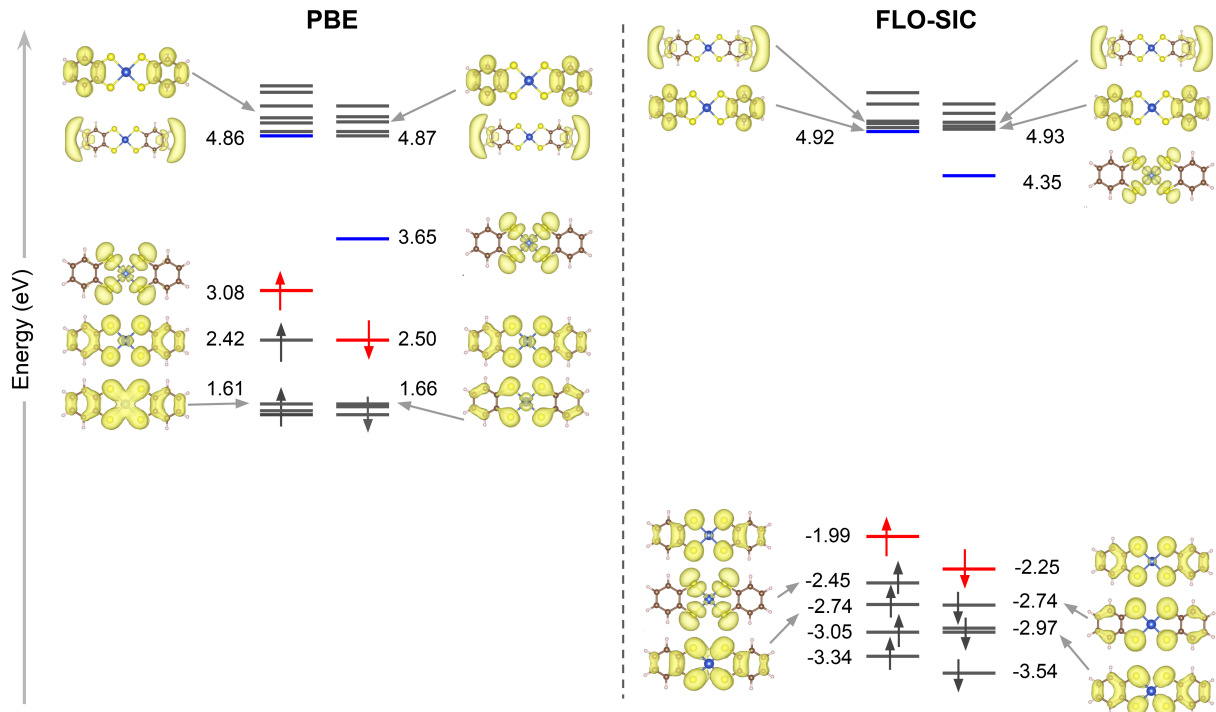


FIG. 7. Energy levels and corresponding canonical orbitals of the **Q-2** molecule from the SIC-free PBE-GGA and FLO-SIC calculations

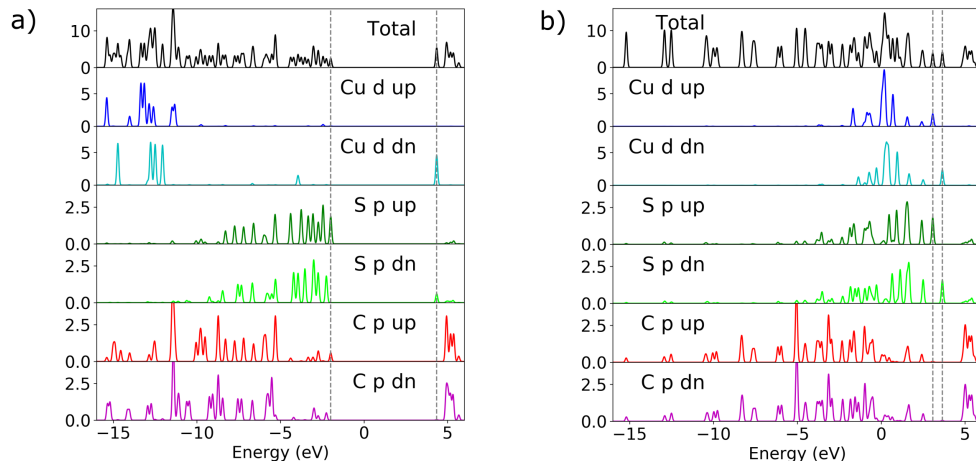


FIG. 8. (a) FLO-SIC and (b) SIC-free DFT calculated densities of states (DOS) projected onto spin-up and spin-down Cu *d*, S *p*, and C *p* orbitals of the **Q-2** molecule where the left and right vertical dashed lines indicate the HOMO and LUMO levels. The FLO-SIC HOMO-LUMO gap is 6.34 eV, while the SIC-free DFT HOMO-LUMO gap is 0.56 eV.

HOMO and LUMO are from the spin-down (minority-spin) channel. The relatively smaller Cu contribution to the spin density (Table II) and the positive HOMO energy (Table III) are consistent with our SIC-free PBE-GGA result. However, these B3LYP results mostly do not agree even qualitatively with the experimental data or our FLO-SIC results. Note that our CASSCF result is not in line with the B3LYP result, either. In

order to reconcile the discrepancy between the EPR experimental data¹⁷ and the B3LYP result and to explain the oxidation pathway to **Q-1**, Ref. 17 alternatively proposed co-existence of the two competing iso-electronic states for **Q-2** using TDDFT: $[\text{Cu}^{\text{I}}(\text{bdt}_2, 4\text{S}^{3-*})]^{2-}$ and $[\text{Cu}^{\text{II}}(\text{bdt}_2, 4\text{S}^{4-})]^2$. In the former, the four S atoms give rise to spin $S = 1/2$, while in the latter the Cu atom carries one unpaired electron. Our FLO-SIC results and

multiconfigurational/multireference calculations as well as experimental data¹⁶ support the latter state rather than the proposed co-existent states.

V. FLO-SIC RESULTS FOR THE Q-1 MOLECULE

Our SIC-free DFT calculations and experiments¹⁷ on **Q-1** suggest that the singlet state has a lower energy than the triplet state. Therefore, we consider only the singlet state in the FLO-SIC calculations.

A. Converged FODs

The FLO-SIC procedure for studies of the **Q-1** molecule is similar to that described for **Q-2**. Since we carry out spin-unpolarized FLO-SIC calculations, the total number of FODs is now reduced to 87. We start with 4 initial spin-unpolarized FOD configurations as illustrated in Fig. 4, similarly to the case of **Q-2**. We converge the 4 initial FOD configurations through 6 individual frozen-density loop cycles. Table IV lists the converged total energies and maximum force components after the 6 cycles. FOD configuration 2 gives the lowest energy, but the energy differences among the different FOD configurations are on the order of 0.1 mHa. The maximum force component F_{\max} is about 1 mHa/ a_B , while the maximum electric dipole moment component is about 0.009-0.01 in atomic units. The dipole moment is slightly larger than that for the **Q-2** molecule, which is consistent with the fact that the molecular geometry of **Q-1** was optimized without symmetry constraints. The converged FODs of configuration 2 are shown in Fig. 9 and the FOD positions are listed in the Appendix C 2 (Table X). We confirm that the FLO-SIC electronic structure from the other converged FOD configurations 1, 3, and 4 is very close to that from the converged FOD configuration 2, within our numerical accuracy (see Table XII in the Appendix D), although the final FOD configurations are somewhat different from one another. Henceforth, we analyze the FLO-SIC electronic structure obtained from the converged FOD configuration 2. Again, we check that the electronic structure does not change with further FOD relaxations or with further decrease of the dipole moment.

B. FLO-SIC calculated electronic structure

Table V shows the energies of the HOMO and LUMO of the **Q-1** molecule calculated from the FLO-SIC method. We find that the HOMO energy is -5.90 eV, which is 3.91 eV lower than the HOMO energy of the **Q-2** molecule. The SIC shifts the HOMO (LUMO) level downward by 4.61 (0.67) eV in comparison to the SIC-free DFT results, such that it increases the HOMO-LUMO gap to 4.68 eV.

TABLE IV. Converged SCF total energies E and maximum final force components F_{\max} after the 6 frozen-density loop cycles, and energy differences ΔE between the 6-th and 5-th frozen-density loops for configuration 1-4 (labeled in Fig. 4) of the **Q-1** molecule. Each frozen-density loop consists of many FOD updates.

FOD Conf	E (Ha)	F_{\max} (mHa/ a_B)	ΔE (mHa)
1	-3703.29260	0.35	-0.75
2	-3703.29262	0.34	-0.89
3	-3703.29231	0.28	-2.10
4	-3703.29250	0.38	-1.04

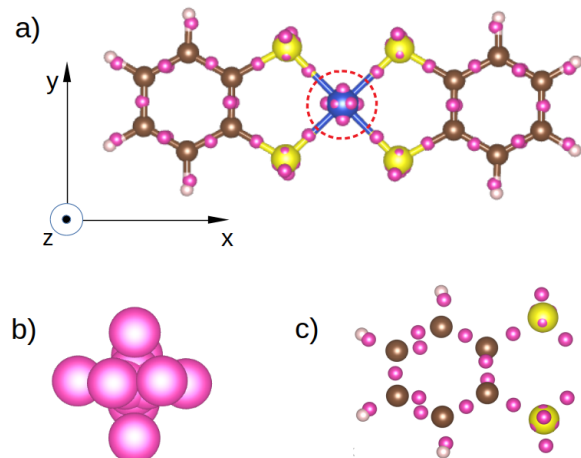


FIG. 9. (a) Converged spin-unpolarized FOD positions from configuration 2 for the **Q-1** molecule. (b) Zoom-in of the FODs near the Cu atom and (c) zoom-in of the FODs near the ligands.

TABLE V. Contributions of the Cu d , all S p , and all C p orbitals to the HOMO and LUMO of the **Q-1** (charge $Q = -1$, $S = 0$) molecule calculated using the FLO-SIC method compared to our SIC-free PBE-GGA calculation as well as two B3LYP results^{17,18}. In the former B3LYP calculation, the orbital decomposition was not quantified, while the latter B3LYP result is for a monoanionic Cu-based molecule with similar (slightly different) ligands, $[\text{Cu(III)}(\text{C}_{14}\text{H}_{20}\text{S}_2)_2]^{1-}$,¹⁸ where the HOMO and LUMO energies were not reported. See Fig. 10) for the HOMO and LUMO from the FLO-SIC and PBE-GGA calculations.

Method	Level	Energy(eV)	Cu d	S p	C p
FLO-SIC	HOMO	-5.90	1.6%	67%	31%
	LUMO	-1.22	68%	27%	0.8%
PBE-GGA	HOMO	-1.29	15%	60%	24%
	LUMO	-0.75	43%	51%	1.7%
B3LYP ¹⁷	HOMO	~ -1.5	-	-	-
	LUMO	~ -0.5	-	-	-
B3LYP ¹⁸	HOMO	-	11%	58%	27%
	LUMO	-	33%	58%	4%

Figure 10 shows the HOMO and LUMO and a few

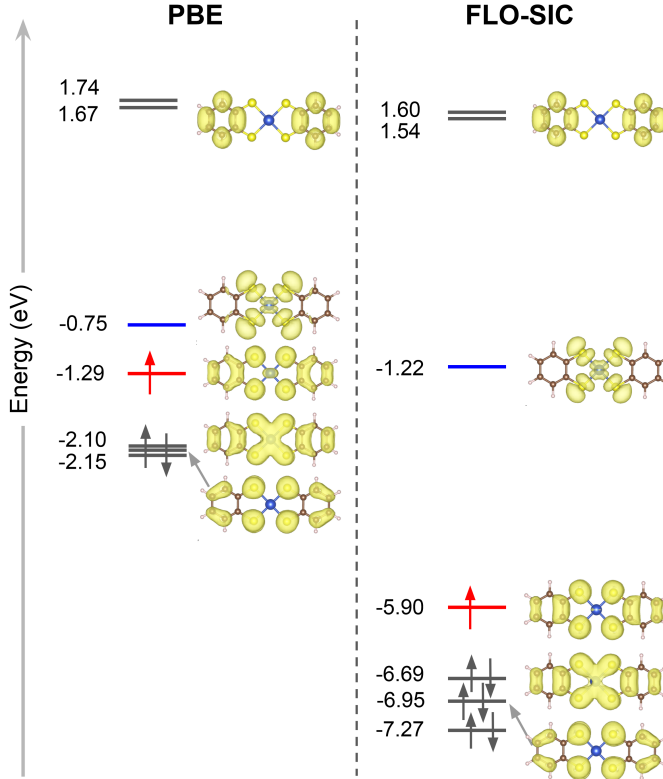


FIG. 10. Energy levels and corresponding canonical orbitals of the **Q-1** molecule from the FLO-SIC and SIC-free PBE-GGA calculations

other *canonical* orbitals of the **Q-1** molecule calculated from the FLO-SIC method compared to the SIC-free PBE-GGA orbitals. The overall orbital shapes do not change much upon the FLO-SIC. The FLO-SIC calculation shows that the major contributions to the HOMO originate from the S p_z and C p_z orbitals at a ratio of almost 2:1 with a very small contribution from the Cu d orbitals, while a majority contribution to the LUMO arises from the Cu d_{xy} and S $p_{x,y}$ orbitals with an approximate ratio of 2:1 (see Table V). These characteristics somewhat differ from those of the SIC-free PBE-GGA results where the HOMO carries a significant contribution from the Cu d_{xz} orbitals and the LUMO originates from almost equal contributions of Cu d and S p orbitals. The canonical orbitals away from the HOMO and LUMO from the FLO-SIC method are very similar to those from the SIC-free PBE-GGA (Fig. 10).

We plot the DOS projected onto Cu d , S p , and C p orbitals obtained using the FLO-SIC method and the SIC-free DFT (see Fig. 11). We find that the SIC lowers the occupied S p and C p orbitals by about 5 eV and most of the Cu $3d$ orbitals by 14-15 eV, which is similar to the case of **Q-2**. Interestingly, for the occupied Cu d orbitals hybridized with the ligands, the energy shift by the SIC is smaller, 9 eV. For **Q-1**, the HOMO character obtained from the FLO-SIC is similar to that from the

SIC-free DFT because a much smaller contribution of the Cu d orbitals to the HOMO.

C. Comparison with previous work

We now compare our FLO-SIC calculated results with the previous experimental and theoretical work^{17,18} for **Q-1**. The characteristics and energies of the FLO-SIC HOMO and LUMO are quite different from the B3LYP results¹⁷ (see Table V) which are closer to the SIC-free PBE-GGA calculation. Interestingly, the B3LYP HOMO-LUMO gap for **Q-1** is smaller than that for **Q-2** by about 1 eV. This feature is similar to the FLO-SIC result, although the gap difference is larger in the FLO-SIC case (~ 1.66 eV). The experimental UV-optical absorption spectra¹⁷ show a maximum peak at 398 nm (3.1 eV) for **Q-1** and a peak at 348 nm (3.6 eV) and possible peaks below 270 nm (4.6 eV) for **Q-2**. Although the optical gap is not equivalent to the HOMO-LUMO gap³⁵, it does provide some indication of the gap size. The difference in the observed gaps is thus consistent with the FLO-SIC HOMO-LUMO gap being smaller in **Q-1**. Our results are also compared with the monoanionic Cu-based molecule with similar (slightly different) ligands such as $[\text{Cu(III)}(\text{C}_{14}\text{H}_{20}\text{S}_2)_2]^{1-18}$. A previous B3LYP DFT calculation¹⁸ on this monoanionic molecule with the scalar relativistic zero-order regular approximation (ZORA) showed that the HOMO consists of Cu d_{xz} (11%), S p_z (58%), and C p_z (27%), while the LUMO consists of Cu d_{xy} (33%), S p_z (58%), and C p_z (4%). Despite slightly different ligands, this orbital decomposition is consistent with our SIC-free PBE-GGA result (see Table V).

VI. CONCLUSIONS AND OUTLOOK

We have investigated the dianionic and monoanionic states of the mononuclear Cu-based molecule which has potential applications for quantum information science, using the FLO-SIC method. Starting with the SIC-free DFT-converged electron density and with multiple initial sets of FODs within the frozen-density loop approach, we determined optimal FLOs with which the SIC energy was obtained self-consistently. Although different initial sets of FODs converged to somewhat different final FOD positions (core and valence FODs), the electronic and magnetic properties obtained from the multiple final converged FODs are very similar to one another within our numerical accuracy. This may suggest an importance of the starting electron density in the FLO-SIC calculations.

As expected, the SIC potential in the FLO-SIC method remedies the severe delocalization of electric charge and spin density caused by the SIE. The FLO-SIC calculations show that in the dianionic case, about 67% of the spin density arises from the Cu d orbitals and about 33% of the spin density is from the S p orbitals. This feature

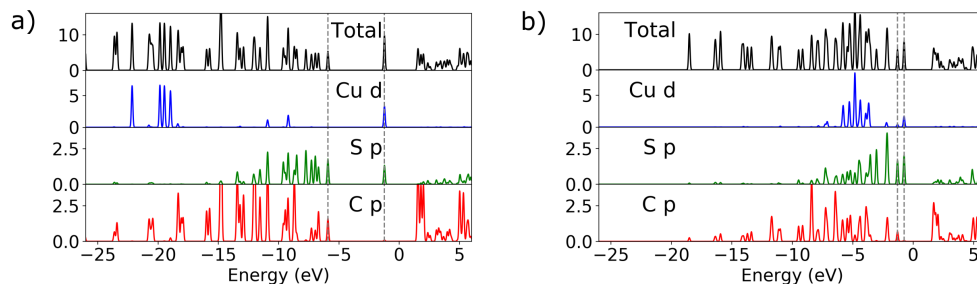


FIG. 11. (a) FLO-SIC and (b) SIC-free DFT calculated densities of states (DOS) projected onto the Cu d , S p , and C p orbitals of the **Q-1** molecule where the left and right vertical dashed lines indicate the HOMO and LUMO levels. The FLO-SIC HOMO-LUMO gap is 4.68 eV, while the SIC-free DFT HOMO-LUMO gap is 0.54 eV.

quantitatively agrees with the multireference result¹⁶ and our multiconfigurational calculation, while the SIC-free PBE-GGA and B3LYP functionals severely underestimate the spin density of the Cu d orbitals. The trend that we found needs to be checked for other transition-metal based molecules with covalent or ionic metal-ligand bonding. It is known that discrepancy between experimental and DFT exchange coupling constants in 3d transition-metal systems, especially overestimation (without sign flip), may be mainly attributed to highly delocalized spin density of the transition-metal d orbitals³⁶. Considering this, our results suggest that the FLO-SIC method may be overall effective in accurately describing the magnetic exchange coupling between 3d transition metal centers within multinuclear magnetic systems^{11,13}.

The SIC potential lowers the energies of the Cu d orbitals by a large amount, which ended up with large changes of the HOMO character compared to the SIC-free DFT result. Whether the FLO-SIC HOMO character is adequate or not requires further studies using more advanced FLO-SIC methods. Utilization of complex orbitals in FLO-SIC calculations^{37,38} may improve the FOD optimization process and provide a better description of systems involving transition metals. It is shown that local scaling SIC appears important in preventing overcorrection of some properties such as polarizabilities and atomization energies³⁹. However, there has been so far no studies of the local scaling SIC effect on the characteristics of the HOMO, which would be also interesting to investigate.

ACKNOWLEDGMENTS

This work was funded by the Department of Energy Basic Energy Sciences grant numbers DE-SC0019033 and DE-SC0018331. The computational support was provided by the Virginia Tech Advanced Research Computing and the Extreme Science and Engineering Discovery Environment (XSEDE) under Project number DMR060009N, which is supported by the National Science Foundation Grant number ACI-1548562. We are

grateful to Mark Pederson, Tunna Baruah, and Rajendra Zope for their extensive help in using and troubleshooting the FLOSIC code. We are also grateful to Kai Trepte for the discussion and for providing us with the frozen-density loop functionality and the fodMC code, and we thank Aleksander Wysocki for helping us set up the CASSCF calculation.

DATA AVAILABILITY

The data that support the findings of this study are available within the article and the Appendices.

Appendix A: Molecular Geometries

1. Dianionic molecule (**Q-2**)
2. Monoanionic molecule (**Q-1**)

Appendix B: CASSCF and UHF calculations for **Q-2**

We perform CASSCF calculations of the **Q-2** molecule in the doublet state ($S = 1/2$) with the active space consisting of 11 electrons and 11 orbitals using *ab-initio* code MOLCAS version 8.2⁴⁰. The 11 active orbitals comprise five Cu 3d orbitals, five Cu 4d (or *d-shell) orbitals, and one Cu-S bonding orbital. Among the five Cu 3d orbitals, one Cu-S antibonding orbital is included. The total number of electrons in the active space is counted considering the doubly occupied Cu-S bonding orbital (Cu 3d_{xy} and S 3p_{x,y}) and nine electrons from the five Cu 3d. The 11 active molecular orbitals with their state-averaged occupation numbers are shown in Fig. 12. Scalar relativistic effects are included based on the Douglas-Kroll-Hess Hamiltonian^{41,42} using relativistically contracted atomic natural orbital (ANO-RCC) basis sets^{43,44}. For all elements, we use the valence double- ζ quality (ANO-RCC-VDZ) basis sets provided in MOLCAS code. Considering the five possibilities of creating a hole in the 3d

TABLE VI. Geometry of the dianionic Cu-based molecule in units of a_B .

Species	x	y	z
Cu	0.0000	0.0000	0.0000
S	-3.0951	-3.0344	0.0000
S	-3.0190	3.0345	0.0000
S	3.0952	3.0345	0.0000
S	3.0191	-3.0344	0.0000
C	-5.9033	-1.2856	-0.1936
C	-5.8796	1.3796	-0.1871
C	-10.4423	1.4295	-0.5952
C	-8.2349	-2.5282	-0.3794
C	-8.1540	2.6950	-0.3968
C	-10.4902	-1.1919	-0.5795
C	5.9034	1.2857	0.1936
C	5.8797	-1.3794	0.1872
C	10.4424	-1.4294	0.5952
C	8.2350	2.5284	0.3794
C	8.1540	-2.6948	0.3968
C	10.4903	1.1920	0.5795
H	-12.1979	2.4933	-0.7648
H	-8.2819	-4.5875	-0.3674
H	-8.1318	4.7546	-0.4054
H	-12.2829	-2.1959	-0.7228
H	12.1981	-2.4933	0.7647
H	8.2820	4.5877	0.3675
H	8.1319	-4.7545	0.4054
H	12.2830	2.1960	0.7228

TABLE VII. Optimized geometry of the monoanionic Cu-based molecule in units of a_B .

Species	x	y	z
Cu	0.0000	0.0000	0.0000
S	-2.9880	-2.9518	-0.0110
S	-2.9198	3.0322	-0.0118
S	2.9882	2.9518	0.0110
S	2.9199	-3.0323	0.0119
C	-5.8516	-1.2592	-0.2332
C	-5.8220	1.4049	-0.2436
C	-10.4096	1.4425	-0.5731
C	-8.1679	-2.5462	-0.3861
C	-8.1134	2.7386	-0.4114
C	-10.4360	-1.2061	-0.5607
C	5.8517	1.2592	0.2332
C	5.8221	-1.4050	0.2436
C	10.4096	-1.4425	0.5730
C	8.1680	2.5461	0.3861
C	8.1136	-2.7387	0.4113
C	10.4361	1.2060	0.5607
H	-12.1754	2.5014	-0.7241
H	-8.1697	-4.6106	-0.3740
H	-8.0702	4.8022	-0.4181
H	-12.2161	-2.2373	-0.7134
H	12.1755	-2.5014	0.7241
H	8.1698	4.6106	0.3740
H	8.0703	-4.8023	0.4181
H	12.2161	2.2373	0.7134

orbitals, we carried out the state average over 5 roots.

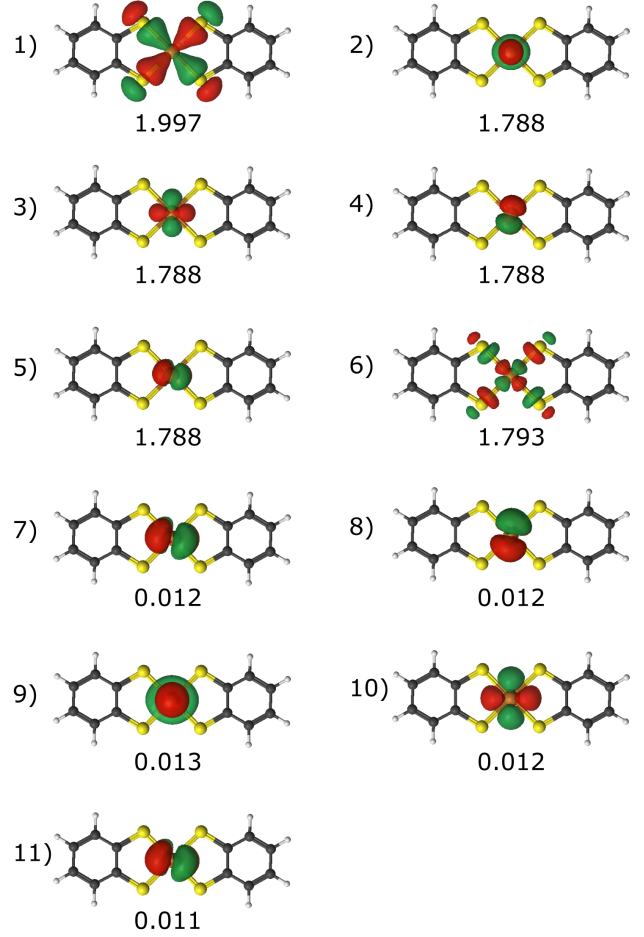


FIG. 12. Molecular orbitals (MO) and state-averaged occupation numbers in the active space for our CASSCF(11,11) calculation of the **Q-2** molecule. The ground-state configuration consists of doubly occupied MO 1-5, singly occupied MO 6, and empty MO 7-11.

From the CASSCF(11,11) calculations, we find that the ground state (lowest-energy root) has a configuration of the doubly occupied Cu-S bonding orbital (MO 1: Cu $3d_{xy}$ and S $3p_{x,y}$), the four doubly occupied Cu $3d$ orbitals (MO 2-5: d_{z^2} , $d_{x^2-y^2}$, d_{yz} , d_{xz}), the singly occupied Cu-S antibonding orbital (MO 6: Cu $3d_{xy}$ and S $3p_{x,y}$), and empty Cu $4d$ orbitals (MO 7-11).

Unrestricted Hartree-Fock (UHF) calculations are performed for the **Q-2** molecule in the doublet state ($S = 1/2$) using MOLCAS version 8.2⁴⁰. We use ANO-RCC-VDZ basis sets for all the atoms.

Appendix C: Converged FOD Geometries

1. Dianionic molecule: FOD Configuration 4

TABLE VIII: Converged geometry of spin-up FODs (configuration 4) for **Q-2** in units of a_B .

Spin UP			
Orb. Type	x	y	z
Cu 1s	0.000000	0.000000	0.000000
Cu 2sp	0.140437	-0.006153	0.121301
	-0.147459	0.008121	0.111994
	0.011429	0.166278	-0.123538
	-0.004199	-0.168263	-0.121273
Cu 3spd	0.533382	0.563552	0.363919
	-0.548512	-0.557042	0.344983
	-0.500887	0.606451	0.338860
	0.483260	-0.600871	0.370400
	0.721904	-0.035822	-0.585479
	-0.694333	0.026664	-0.625292
	0.027308	0.407041	-0.382308
	-0.008506	-0.412614	-0.377110
	-0.015814	0.004469	0.728797
	-2.111473	-1.842142	0.068512
Cu-S bonds	-2.076545	1.810656	0.109787
	2.099305	1.864911	0.265062
	2.068580	-1.828072	0.242089
	-3.095100	-3.034400	0.000000
Ligands	-3.101429	-2.765981	-0.391111
	-2.723407	-3.305934	0.045615
	-3.429507	-3.361022	0.015010
	-3.128710	-2.693342	0.330667
	-4.562630	-2.068162	-0.111434
	-3.208291	-3.910813	-1.368258
	-3.322393	-3.873760	1.378195
	-3.019000	3.034500	0.000000
	-3.056048	2.695316	0.332578
	-2.644963	3.302568	0.042083
	-3.025741	2.766809	-0.391055
	-3.352441	3.361822	0.017076
	-4.515427	2.118259	-0.105528
	-3.208008	3.914183	1.359502
	-3.085594	3.878898	-1.394130
	-5.903300	-1.285600	-0.193600
	-5.834331	0.047515	-1.226000
	-6.046157	0.049012	0.975923
	-7.017290	-2.002031	-0.273916
	-5.879600	1.379600	-0.187100
	-6.963985	2.128132	-0.275508
	-10.442300	1.429500	-0.595200
	-9.253654	1.997210	-1.351158
	-9.399692	1.987056	0.359386
	-10.613748	0.121326	-0.590620
	-11.901501	2.120958	-0.748147
	-8.234900	-2.528200	-0.379400
	-9.324935	-1.804501	-1.340106
	-9.455418	-1.771954	0.364704
	-8.109587	-4.142157	-0.371431
	-8.154000	2.695000	-0.396800
	-7.974475	4.304984	-0.405633
	-10.490200	-1.191900	-0.579500
	-11.975389	-1.834973	-0.715014
	3.095200	3.034500	0.000000
	3.118318	2.776295	0.397660
	2.721877	3.298697	-0.061242
	3.431148	3.358185	-0.005696
	3.112116	2.694790	-0.327862
Continued on the next column			

Continuation of Table VIII			
Orb. Type	x	y	z
	4.567332	2.067120	0.092021
	3.239123	4.127233	1.197780
	3.281845	3.624508	-1.524598
	3.019100	-3.034400	0.000000
	3.036860	-2.694898	-0.329390
	2.644071	-3.296117	-0.061708
	3.044641	-2.776198	0.398150
	3.354005	-3.359786	-0.004370
	4.517107	-2.116384	0.083802
	3.183481	-3.654536	-1.512668
	3.105700	-4.110867	1.215247
	5.903400	1.285700	0.193600
	5.855322	-0.047856	1.271607
	6.013191	-0.048392	-0.924280
	7.016180	2.002949	0.282524
	5.879700	-1.379400	0.187200
	6.963033	-2.128481	0.284354
	10.442400	-1.429400	0.595200
	9.247638	-1.983879	1.356095
	9.406294	-1.999631	-0.356898
	10.611694	-0.121133	0.600671
	11.901929	-2.122664	0.730683
	8.235000	2.528400	0.379400
	9.318521	1.791676	1.345438
	9.462484	1.784652	-0.362645
	8.111172	4.141376	0.353021
	8.154000	-2.694800	0.396800
	7.976123	-4.304237	0.387162
	10.490300	1.192000	0.579500
	11.975580	1.836666	0.697490

TABLE IX: Converged geometry of spin-down FODs (configuration 4) for **Q-2** in units of a_B .

Spin DOWN			
Orb. Type	x	y	z
Cu 1s	0.000000	0.000000	0.000000
Cu 2sp	0.130298	-0.027391	-0.156584
	-0.174223	-0.026294	-0.059652
	0.016902	0.176076	0.058717
	0.031878	-0.127228	0.157324
Cu 3spd	0.840120	0.011401	0.249996
	-0.755827	-0.015060	0.262829
	-0.034422	0.415893	0.654691
	0.011549	-0.310753	0.473532
	0.310661	-0.011339	-0.470749
	-0.421930	0.035834	-0.668717
	0.012690	0.749680	-0.259756
	-0.003356	-0.840355	-0.247173
Cu-S bonds	-1.944906	-1.856133	-0.108011
	-1.889778	1.810019	-0.024370
	1.968248	1.831567	0.075125
	1.869221	-1.791551	0.012073
Ligands	-3.095100	-3.034400	0.000000
	-3.104623	-2.792723	-0.399787
	-2.713020	-3.281980	0.047461
	-3.124771	-2.714818	0.339812
	-3.442438	-3.342633	0.012001
Continued on the next column			

Continuation of Table IX			
Orb. Type	x	y	z
	-3.091948	-3.953547	-1.367253
	-3.249423	-3.711402	1.507150
	-3.019000	3.034500	0.000000
	-3.031520	2.795520	-0.397043
	-2.635299	3.275305	0.043065
	-3.050727	2.720721	0.340219
	-3.362062	3.341376	0.013373
	-3.146003	3.787235	1.500560
	-3.013779	3.960913	-1.402001
	-5.903300	-1.285600	-0.193600
	-4.577437	-1.995539	-0.094181
	-5.879600	1.379600	-0.187100
	-4.545042	2.045505	-0.094045
	-5.696598	0.044912	-0.172740
	-10.442300	1.429500	-0.595200
	-8.234900	-2.528200	-0.379400
	-7.105984	-1.905376	-1.234125
	-7.251680	-1.911673	0.660927
	-8.154000	2.695000	-0.396800
	-7.045929	2.032268	-1.250852
	-7.201763	2.052201	0.650728
	-9.338694	2.135280	-0.499804
	-10.490200	-1.191900	-0.579500
	-10.535883	0.126545	0.369795
	-10.359909	0.108835	-1.541474
	-9.405401	-1.931696	-0.482550
	-11.761447	2.344416	-0.719292
	-8.373172	-4.109167	-0.374801
	-8.236908	4.279416	-0.407785
	-11.841502	-2.063441	-0.684648
	3.095200	3.034500	0.000000
	3.099965	2.792682	0.399867
	2.712265	3.281476	-0.043372
	3.129430	2.716851	-0.341432
	3.443544	3.341366	-0.014693
	3.092415	3.916495	1.391044
	3.253715	3.761675	-1.484140
	3.019100	-3.034400	0.000000
	3.028511	-2.795451	0.395219
	2.635777	-3.274514	-0.039840
	3.054223	-2.722745	-0.339478
	3.361099	-3.340366	-0.015591
	3.161725	-3.825869	-1.487450
	3.012624	-3.937765	1.421397
	5.903400	1.285700	0.193600
	4.569765	1.992810	0.093496
	5.879700	-1.379400	0.187200
	4.548281	-2.047422	0.089451
	5.696742	-0.044162	0.173826
	10.442400	-1.429400	0.595200
	8.235000	2.528400	0.379400
	7.103359	1.906668	1.225390
	7.256631	1.910027	-0.670244
	8.154000	-2.694800	0.396800
	7.043586	-2.032815	1.243270
	7.205103	-2.051525	-0.660238
	9.338475	-2.134622	0.499690
	10.490300	1.192000	0.579500
	10.534110	-0.126374	-0.372469
	10.362186	-0.109057	1.541334
	9.405378	1.931580	0.482034
Continued on the next column			

Continuation of Table IX			
Orb. Type	x	y	z
	11.761808	-2.343494	0.721289
	8.372809	4.109440	0.375394
	8.235965	-4.279196	0.407798
	11.841594	2.062818	0.686736

2. Monoanionic molecule: FOD Configuration 2

TABLE X: Converged FOD geometry of configuration 2 for **Q-1** in units of a_B

Orb. Type	x	y	z
Cu 1s	0.000000	0.000000	0.000000
Cu 2sp	0.171963	-0.021944	0.068097
	-0.132286	-0.023862	0.154110
	-0.014376	0.173357	-0.067050
	-0.027987	-0.130181	-0.155197
Cu 3spd	0.394996	0.024379	0.617239
	-0.001482	-0.823311	0.249773
	-0.310798	-0.007790	0.469381
	0.746606	-0.016562	-0.261254
	0.036822	0.396496	-0.614567
	-0.820871	0.023746	-0.252955
	0.003839	0.744894	0.262968
	-0.014743	-0.308952	-0.470619
Cu-S bonds	-1.781915	-1.691625	-0.018311
	-1.791331	1.782652	-0.109085
	1.797969	1.710358	0.008900
Ligands	1.780486	-1.790712	0.093198
	-2.987407	-2.951645	-0.010186
	-3.345872	-3.242831	0.004111
	-2.595029	-3.173913	0.026158
	-3.025560	-2.657471	0.339888
	-2.992640	-2.732125	-0.416618
	-4.531494	-2.019853	-0.133993
	-2.878634	-3.750841	-1.469355
	-3.044755	-3.598620	1.526392
	-2.919038	3.032393	-0.012400
	-2.941888	2.746792	-0.376666
	-2.568019	3.319207	0.041078
	-3.224241	3.386509	0.003995
	-2.952933	2.675032	0.286776
	-4.460880	2.143257	-0.118220
	-3.009789	3.607845	1.520725
	-2.720682	3.775947	-1.449289
	2.988705	2.951802	0.010166
	3.347068	3.240376	-0.003442
	2.991387	2.733508	0.418910
	3.025331	2.658371	-0.342131
	2.591924	3.173543	-0.026491
	4.529326	2.017766	0.138384
	2.876767	3.741768	1.470373
	3.030660	3.589093	-1.525161
	2.920530	-3.032262	0.012655
	3.218776	-3.389315	0.002669
	2.945682	-2.672171	-0.283756
	2.949366	-2.744008	0.373499
Continued on the next column			

Continuation of Table X			
Orb. Type	x	y	z
	2.568700	-3.323262	-0.047971
	4.460029	-2.132216	0.126484
	2.992370	-3.624563	-1.510985
	2.728562	-3.793353	1.438725
	-5.868791	-1.332683	-0.231923
	-5.922333	0.079014	0.794537
	-5.786270	0.069544	-1.306878
	-6.937767	-2.009568	-0.306224
	-5.839102	1.478004	-0.244650
	-6.898334	2.169549	-0.327058
	-10.459506	1.390212	-0.575636
	-9.194208	2.012593	-1.360434
	-9.329891	2.028817	0.374653
	-10.513841	0.119294	-0.572553
	-11.835054	2.173869	-0.687385
	-8.099575	-2.565909	-0.382148
	-9.372209	-1.804942	0.398234
	-9.233172	-1.806713	-1.329643
	-8.025888	-4.128546	-0.360571
	-8.044570	2.756914	-0.406001
	-7.944740	4.321873	-0.402115
	-10.484763	-1.152881	-0.565010
	-11.874154	-1.913766	-0.673746
	5.869096	1.332206	0.231920
	5.925368	-0.080192	-0.804028
	5.783175	-0.070854	1.316307
	6.938917	2.008504	0.304771
	5.839239	-1.478021	0.244374
	6.901224	-2.165487	0.325413
	10.459557	-1.390233	0.575542
	9.328372	-2.027619	-0.377502
	9.193831	-2.013564	1.364061
	10.513699	-0.119602	0.571584
	11.835639	-2.173955	0.689013
	8.099563	2.565841	0.382213
	9.234255	1.807794	1.329987
	9.371656	1.803899	-0.398104
	8.025786	4.128456	0.362188
	8.044535	-2.756844	0.405958
	7.950583	-4.325674	0.404086
	10.484870	1.152872	0.565014
	11.873725	1.914077	0.675239

Appendix D: Final FOD-configuration dependence of HOMO-LUMO gap and spin density for Q-2 and Q-1

TABLE XI. Final FOD dependence of the electronic structure such as the HOMO and LUMO energies, HOMO-LUMO gap, and Mulliken spin population on the Cu and S atoms for **Q-2**. The final converged FOD configurations starting from FOD configuration 2-8 are used for the calculation.

Property	Conf.2	Conf.3	Conf.4	Conf.5	Conf.6	Conf.7	Conf.8
HOMO energy (eV)	-1.99	-1.99	-1.99	-1.99	-1.99	-1.99	-1.99
LUMO energy (eV)	4.35	4.35	4.35	4.37	4.38	4.34	4.34
HOMO-LUMO gap (eV)	6.34	6.34	6.34	6.36	6.37	6.33	6.34
Spin Cu (μ_B)	0.666	0.666	0.665	0.660	0.658	0.670	0.674
Spin S (μ_B)	0.333	0.333	0.334	0.337	0.340	0.326	0.321

TABLE XII. Final FOD dependence of the electronic structure such as the HOMO and LUMO energies and HOMO-LUMO gap for **Q-1**. The final converged FOD configurations starting from FOD configuration 1-4 are used for the calculations.

Property	Conf.1	Conf.2	Conf.3	Conf.4
HOMO energy (eV)	-5.90	-5.90	-5.90	-5.90
LUMO energy (eV)	-1.22	-1.22	-1.22	-1.22
HOMO-LUMO gap (eV)	4.68	4.68	4.68	4.68

- ¹J. P. Perdew and A. Zunger, "Self-interaction correction to density-functional approximations for many-electron systems," *Phys. Rev. B* **23**, 5048–5079 (1981).
- ²V. I. Anisimov, F. Aryasetiawan, and A. I. Lichtenstein, "First-principles calculations of the electronic structure and spectra of strongly correlated systems: the LDA+U method," *Journal of Physics: Condensed Matter* **9**, 767–808 (1997).
- ³H. J. Kulik, M. Cococcioni, D. A. Scherlis, and N. Marzari, "Density functional theory in transition-metal chemistry: A self-consistent Hubbard U approach," *Phys. Rev. Lett.* **97**, 103001 (2006).
- ⁴M. R. Pederson, R. A. Heaton, and C. C. Lin, "Local-density Hartree-Fock theory of electronic states of molecules with self-interaction correction," *The Journal of Chemical Physics* **80**, 1972–1975 (1984), <https://doi.org/10.1063/1.446959>.
- ⁵R. A. Heaton, J. G. Harrison, and C. C. Lin, "Self-interaction correction for density-functional theory of electronic energy bands of solids," *Phys. Rev. B* **28**, 5992–6007 (1983).
- ⁶M. R. Pederson, A. Ruzsinszky, and J. P. Perdew, "Communication: Self-interaction correction with unitary invariance in density functional theory," *The Journal of Chemical Physics* **140**, 121103 (2014), <https://doi.org/10.1063/1.4869581>.
- ⁷M. R. Pederson, "Fermi orbital derivatives in self-interaction corrected density functional theory: Applications to closed shell atoms," *The Journal of Chemical Physics* **142**, 064112 (2015), <https://doi.org/10.1063/1.4907592>.
- ⁸M. R. Pederson, T. Baruah, D.-y. Kao, and L. Basurto, "Self-interaction corrections applied to Mg-porphyrin, C_{60} , and pentacene molecules," *The Journal of Chemical Physics* **144**, 164117 (2016), <https://doi.org/10.1063/1.4947042>.
- ⁹S. Adhikari, B. Santra, S. Ruan, P. Bhattarai, N. K. Nepal, K. A. Jackson, and A. Ruzsinszky, "The Fermi-Löwdin self-interaction correction for ionization energies of organic molecules," *The Journal of Chemical Physics* **153**, 184303 (2020), <https://doi.org/10.1063/5.0024776>.
- ¹⁰J. Vargas, P. Ufondu, T. Baruah, Y. Yamamoto, K. A. Jackson, and R. R. Zope, "Importance of self-interaction-error removal in density functional calculations on water cluster anions," *Phys. Chem. Chem. Phys.* **22**, 3789–3799 (2020).
- ¹¹K. A. Jackson, J. E. Peralta, R. P. Joshi, K. P. Withanage, K. Treppe, K. Sharkas, and A. I. Johnson, "Towards efficient density functional theory calculations without self-interaction: The Fermi-Löwdin orbital self-interaction correction," *Journal of Physics: Conference Series* **1290**, 012002 (2019).
- ¹²A. I. Johnson, K. P. K. Withanage, K. Sharkas, Y. Yamamoto, T. Baruah, R. R. Zope, J. E. Peralta, and K. A. Jackson, "The effect of self-interaction error on electrostatic dipoles calculated using density functional theory," *The Journal of Chemical Physics* **151**, 174106 (2019).
- ¹³R. P. Joshi, K. Treppe, K. P. K. Withanage, K. Sharkas, Y. Yamamoto, L. Basurto, R. R. Zope, T. Baruah, K. A. Jackson, and J. E. Peralta, "Fermi-Löwdin orbital self-interaction correction to magnetic exchange couplings," *The Journal of Chemical Physics* **149**, 164101 (2018), <https://doi.org/10.1063/1.5050809>.
- ¹⁴S. Schwalbe, T. Hahn, S. Liebing, K. Treppe, and J. Kortus, "Fermi-Löwdin orbital self-interaction corrected density functional theory: Ionization potentials and enthalpies of formation," *Journal of Computational Chemistry* **39**, 2463–2471 (2018), <https://onlinelibrary.wiley.com/doi/pdf/10.1002/jcc.25586>.
- ¹⁵D.-y. Kao, M. R. Pederson, T. Hahn, T. Baruah, S. Liebing, and J. Kortus, "The role of self-interaction corrections, vibrations, and spin-orbit in determining the ground spin state in a simple heme," *Magnetochemistry* **3** (2017), 10.3390/magnetochemistry3040031.
- ¹⁶M. S. Fataftah, M. D. Krzyaniak, B. Vlasisavljevic, M. R. Wasielewski, J. M. Zadrozny, and D. E. Freedman, "Metal-ligand covalency enables room temperature molecular qubit candidates," *Chem. Sci.* **10**, 6707–6714 (2019).
- ¹⁷B. K. Maiti, L. B. Maia, K. Pal, B. Pakhira, T. Avilés, I. Moura, S. R. Pauleta, J. L. Nuñez, A. C. Rizzi, C. D. Brondino, S. Sarkar, and J. J. G. Moura, "One electron reduced square planar bis(benzene-1,2-dithiolato) copper dianionic complex and redox switch by O_2/HO^- ," *Inorganic Chemistry* **53**, 12799–12808 (2014), pMID: 25470763, <https://doi.org/10.1021/ic501742j>.
- ¹⁸K. Ray, T. Weyhermüller, F. Neese, and K. Wieghardt, "Electronic structure of square planar bis(benzene-1,2-dithiolato)metal complexes $[M(L)_2]^z$ ($z = 2-, 1-, 0$; $m = Ni, Pd, Pt, Cu, Au$): An experimental, density functional, and correlated ab initio study," *Inorganic Chemistry* **44**, 5345–5360 (2005).
- ¹⁹N. Robertson and L. Cronin, "Metal bis-1,2-dithiolene complexes in conducting or magnetic crystalline assemblies," *Coordination Chemistry Reviews* **227**, 93–127 (2002).
- ²⁰D.-y. Kao, K. Withanage, T. Hahn, J. Batool, J. Kortus, and K. Jackson, "Self-consistent self-interaction corrected density functional theory calculations for atoms using Fermi-Löwdin orbitals: Optimized Fermi-orbital descriptors for Li–Kr," *The Journal of Chemical Physics* **147**, 164107 (2017), <https://doi.org/10.1063/1.4996498>.
- ²¹J. P. Perdew, K. Burke, and M. Ernzerhof, "Generalized gradient approximation made simple," *Phys. Rev. Lett.* **77**, 3865–3868 (1996).
- ²²M. R. Pederson and K. A. Jackson, "Variational mesh for quantum-mechanical simulations," *Phys. Rev. B* **41**, 7453–7461 (1990).
- ²³K. Jackson and M. R. Pederson, "Accurate forces in a local-orbital approach to the local-density approximation," *Phys. Rev. B* **42**, 3276–3281 (1990).
- ²⁴M. Pederson, D. Porezag, J. Kortus, and D. Patton, "Strategies for massively parallel local-orbital-based electronic structure methods," *physica status solidi (b)* **217**, 197–218 (2000).
- ²⁵Z.-h. Yang, M. R. Pederson, and J. P. Perdew, "Full self-consistency in the Fermi-orbital self-interaction correction," *Phys. Rev. A* **95**, 052505 (2017).
- ²⁶P.-O. Löwdin, "On the non-orthogonality problem connected with the use of atomic wave functions in the theory of molecules and crystals," *The Journal of Chemical Physics* **18**, 365–375 (1950), <https://doi.org/10.1063/1.1747632>.
- ²⁷R. Zope, T. Baruah, and K. A. Jackson, *FLOSIC 0.2, based on the NRLMOL code of M. R. Pederson*.
- ²⁸D. Porezag and M. R. Pederson, "Optimization of Gaussian basis sets for density-functional calculations," *Phys. Rev. A* **60**, 2840–2847 (1999).
- ²⁹J. P. Perdew and Y. Wang, "Accurate and simple analytic representation of the electron-gas correlation energy," *Phys. Rev. B* **45**, 13244–13249 (1992).
- ³⁰S. Schwalbe, K. Treppe, L. Fiedler, A. I. Johnson, J. Kraus, T. Hahn, J. E. Peralta, K. A. Jackson, and J. Kortus, "Interpretation and automatic generation of Fermi-orbital descriptors," *Journal of Computational Chemistry* **40**, 2843–2857 (2019), <https://onlinelibrary.wiley.com/doi/pdf/10.1002/jcc.26062>.
- ³¹A. D. Becke, "Density-functional thermochemistry. iii. the role of exact exchange," *The Journal of Chemical Physics* **98**, 5648–5652 (1993), <https://doi.org/10.1063/1.464913>.
- ³²C. Lee, W. Yang, and R. G. Parr, "Development of the Colle-Salvetti correlation-energy formula into a functional of the electron density," *Phys. Rev. B* **37**, 785–789 (1988).
- ³³S. H. Vosko, L. Wilk, and M. Nusair, "Accurate spin-dependent electron liquid correlation energies for local spin density calculations: a critical analysis," *Canadian Journal of Physics* **58**, 1200–1211 (1980).
- ³⁴P. J. Stephens, F. J. Devlin, C. F. Chabalowski, and M. J. Frisch, "Ab initio calculation of vibrational absorption and circular dichroism spectra using density functional force fields," *The Journal of Physical Chemistry* **98**, 11623–11627 (1994).
- ³⁵J.-L. Bredas, "Mind the gap!" *Mater. Horiz.* **1**, 17–19 (2014).
- ³⁶I. Rudra, Q. Wu, and T. Van Voorhis, "Accurate magnetic exchange couplings in transition-metal complexes from constrained density-functional theory," *The Journal of Chemical Physics* **124**, 024103 (2006).

- ³⁷S. Klüpfel, P. Klüpfel, and H. Jónsson, “Importance of complex orbitals in calculating the self-interaction-corrected ground state of atoms,” *Phys. Rev. A* **84**, 050501 (2011).
- ³⁸S. Lehtola, M. Head-Gordon, and H. Jónsson, “Complex orbitals, multiple local minima, and symmetry breaking in Perdew-Zunger self-interaction corrected density functional theory calculations,” *Journal of Chemical Theory and Computation* **12**, 3195–3207 (2016).
- ³⁹S. Romero, Y. Yamamoto, T. Baruah, and R. R. Zope, “Local self-interaction correction method with a simple scaling factor,” *Phys. Chem. Chem. Phys.* **23**, 2406–2418 (2021).
- ⁴⁰F. Aquilante, J. Autschbach, R. Carlson, L. Chibotaru, M. Delcey, L. De Vico, I. Galván, N. Ferré, L. Frutos, L. Gagliardi, M. Garavelli, A. Giussani, C. Hoyer, G. Li Manni, H. Lischka, D. Ma, P.-Å. Malmqvist, T. Mueller, A. Nenov, and R. Lindh, “Molcas 8: New capabilities for multiconfigurational quantum chemical calculations across the periodic table,” *Journal of computational chemistry* **37** (2015), 10.1002/jcc.24221.
- ⁴¹M. Douglas and N. M. Kroll, “Quantum electrodynamical corrections to the fine structure of helium,” *Ann. Phys.* **82**, 89–155 (1974).
- ⁴²B. A. Hess, “Relativistic electronic-structure calculations employing a two-component no-pair formalism with external-field projection operators,” *Phys. Rev. A* **33**, 3742–3748 (1986).
- ⁴³P.-O. Widmark, P.-Å. Malmqvist, and B. O. Roos, “Density matrix averaged atomic natural orbital (ano) basis sets for correlated molecular wave functions,” *Theor. Chem. Acc.* **77**, 291–306 (1990).
- ⁴⁴B. O. Roos, R. Lindh, P.-Å. Malmqvist, V. Veryazov, and P.-O. Widmark, “Main group atoms and dimers studied with a new relativistic ano basis set,” *J. Phys. Chem. A* **108**, 2851–2858 (2004).